Calculation of pressure- and migration-constrained dynamic CO_2 storage capacity of the North Sea Forties and Nelson dome structures

Masoud Babaei[1*], Rajesh Govindan[2], Anna Korre[2], Ji-Quan Shi[2], Sevket Durucan[2] and Martyn Quinn[3]

[1]School of Chemical Engineering and Analytical Science, University of Manchester, Manchester M13 9PL, United Kingdom

[2]Department of Earth Science and Engineering, Royal School of Mines, Imperial College London, London SW7 2BP, United Kingdom

[3]British Geological Survey, The Lyell Centre, Edinburgh EH14 4AP, United Kingdom

Abstract

This paper presents a numerical simulation study of CO_2 injection into the Forties and Nelson dome structures in the North Sea. The study assumes that these structures are fully depleted of their remaining hydrocarbon and brine has replaced their pore space, and therefore the structures can be treated as saline aquifers. Under this assumption, the objective is to calculate the dynamic CO_2 storage capacity of the Forties and Nelson structures and design an injection scenario to enhance storage utilisation. In doing so, first, a detailed geological model of the dome structures and their surrounding aquifer is developed to represent the lithological facies associations and attribute them with petrophysical properties. The geological model is calibrated in terms of the surrounding aquifer support using the hydrocarbon production data. The dynamic storage capacity is subsequently estimated by numerical simulation of the two-phase (brine and CO_2) process. Key performance indicators (KPIs), such as the pressure build-up and regional mass fraction of CO_2, are used to constrain the injection scenarios that consequently result in the best capacity utilisation of the storage structures. In our model of fully brine saturated dome structures, based on specific constraints, namely <0.1% of the total gaseous CO_2 outside the dome into an upper pressure unit and 66% of the initial hydrostatic pressure as the allowable increase in the bottom-hole pressure, we obtained a dynamic capacity of 121 million tonnes for the Forties structure and 24 million tonnes for the Nelson structure. These values are subject to change when a three phase model of residual oil, gas and water is considered in simulations.

1. Introduction

The storage of carbon dioxide in depleted or mature oil or natural gas reservoirs has obvious advantages over storage in pristine aquifers where we have a limited and uncertain knowledge of the geological environment, namely their trapping potential or storage capacity. Porous rock formations that are proven traps have retained hydrocarbons for millions of years, and are potential candidates for CO_2 storage (IPCC, 2005). Moreover, this option may even be economically sustainable as it can enhance oil or gas recovery (EOR/EGR). Hence, CO_2 injection operations in mature reservoirs are the ones most likely to be implemented first, because of the additional economic benefit that will help offset the cost of CO_2 storage (Holt et al., 1995; Stevens et al., 2000).

Two reservoirs that have been considered for potential CO_2 storage through EOR in the UK Sector of the Central North Sea are the Forties and Nelson oilfields (Espie, 2001; Cawley et al., 2005; SCCS, 2009) which feature high-quality channel sands. Previously, Ketzer et al. (2005) evaluated the long term CO_2 leakage risk from the Forties reservoir assuming that it was filled with supercritical CO_2.

* Corresponding author: The University of Manchester, School of Chemical Engineering and Analytical Science, masoud.babaei@manchester.ac.uk, t: +44 (0)161 306 4554

They reported that the CO_2 plume would travel only a small distance in the overburden during the post-injection period. Cawley et al. (2005) reported that after the injection of CO_2 into the depleted Forties Field, CO_2 would not exceed the capillary entry pressure of the overburden. They also reported that, due to the absence of major faults, the thickness of the reservoir and very low permeability of its overburden, the Forties Field is an ideal structure for CO_2 storage. In none of these studies, however, has a storage capacity estimation of the Forties Field and the neighbouring Nelson Field been presented, where the pressure communication and fluid migration between the two structures that form a part of Forties Sandstone Member are considered in storage performance assessments.

Against this backdrop, we conduct a study in this paper, relying on a large and complex geological model of the two structures in communication with their surrounding aquifer, to estimate the dynamic capacity estimates of the Forties and Nelson fields, assuming that the structures could be treated as saline aquifers. This assumption, which may be unrealistic, is made because our three-phase simulations of the CO_2 injection into the geological model had convergence issues and required prohibitive computational power. Consequently, the results of this work may serve as crude and approximate estimates for the static and dynamic storage capacities of the Forties and Nelson structures neglecting the three-phase complexities and differences with two-phase systems, and provide dynamic capacity estimates of the storage in comparison to the reported static estimates for the same structures. Examples in the literature of presented estimates are SCCS (2009) that reported 138 million tonnes CO_2 capacity for the Forties oilfield by the CO_2-EOR process. Assuming a range of 0.2%–2% storage efficiency, they reported storage capacities of 886–8,856 million tonnes CO_2. Elsewhere, Espie (2001) reported that at least 75 million tonnes of CO_2 could be stored underground as a result of EOR in the Forties Field, with further potential if storage was continued for its own sake after EOR.

In this paper we will use the numerical simulation as the most sophisticated method of estimating dynamic CO_2-storage capacity. Examples of dynamic methods are decline-curve analysis (Frailey, 2009), material balance (Mathias *et al*., 2009; Zhou *et al*., 2008), and reservoir simulation-based approaches (e.g., Doughty and Pruess, 2004; Kumar *et al*. 2004; Ennis-King and Paterson, 2005; Ozah *et al*., 2005; Flett *et al*., 2007; Yamamoto *et al*., 2009 and Liao *et al*., 2014). A full review of the dynamic storage capacity estimation in comparison with static methods is presented in Bachu *et al.* (2015). The numerical methods have the advantage of being able to take into account the heterogeneity of the storage site and trapping of CO_2 by various storage mechanisms that are involved in the storage process. They also account for the physical processes which are important for CO_2 storage, such as the build-up of pressure in the near-well region and throughout the storage site, and migration of CO_2 by advection and buoyancy. Birkholzer et al. (2015) thoroughly surveyed pressure build-up issue and its direct implications on utilizing the storage capacity.

We will use the pressure build-up and migration that may critically affect the storage capacity of aquifer structures to define key performance indicators (KPI's) to assess the injection process as well as to define constrained injection strategies. We will use a novel injectivity-index-weighted dynamic apportioning of rate between a series of fixed injection wells. Injectivity and its dynamic variations are assumed as important factors to be considered in the optimal design of storage capacity utilization (van der Meer and Egberts, 2008; Burton et al., 2008; van der Meer and Yavuz, 2009). The methodology proposed here takes into account effects of the geological model properties on the wells' injectivities and the inflow performances, and dynamic variations of injectivities. Migration and pressure build-up control measures are also simultaneously applied to produce a set of dynamically varying injection rates so that an optimal injection scenario can be designed.

Outline: In the sections that follow, first we describe the geological model of the dome structures in Section 2 (with extra information about the geological settings and model construction in the

Appendix). Next in Section 3, a calibration exercise is presented in which the aquifer support of the study area is adjusted using the pressure behaviour of the hydrocarbon reservoirs. In Section 4, the KPI's are defined and the methodology to extract injection rates based on the dynamically varying injectivity of the injection wells is presented. The results are given in Section 5 and conclusions and future work in Section 6.

2. Study area and geological model

The study area is located on the Forties-Montrose High in the UK Central North Sea (Figure 1a). The 3D model has been built around an area that includes the Forties and Nelson hydrocarbon fields that are four-way dip closed structures containing sandstone reservoirs capped by a thick mudstone-dominated seal. There are four main production platforms, evenly spaced over the area of the Forties field: Forties Alpha (FA), Bravo (FB), Charlie (FC) and Delta (FD), and an auxiliary platform Forties Echo (FE) (Figure 1b). There is only one platform for the Nelson reservoir which is referred to as N in DECC's database for production wells in the North Sea (DECC, 2007). The depth map of the top surface of the 3D model is shown in Figure 1c.

The hydrocarbon reservoirs of the Forties and Nelson fields are submarine fan deposits contained in the Upper Paleocene/ Lower Eocene Sele Formation and overlain by Lower Eocene shales (Hughes *et al*., 1990; Whyatt *et al*., 1992). The reservoirs are located in the proximal inner (interbedded sand/shale) to middle (mainly massive sand) fan region (Hughes *et al*., 1990) and are mostly channelised and characterised by high net to gross ratios, good porosities and high permeabilities (Hempton *et al*., 2005). Detailed geological modelling of the Forties and Nelson hydrocarbon fields in the UK sector of the North Sea has been reported by Kulpecz and van Geuns (1990) and Kunka *et al*. (2003).

The geological model developed in this study broadly captures and represents the heterogeneities present within what is a very complex submarine fan environment. The fan system within the two fields comprises the main hydrocarbon producing fairways: large amalgamated stacked channel systems of the Late Paleocene/ Early Eocene Forties Sandstone Member within four-way dip-closed anticlinal structures. Along with the channels are the associated channel margins and interchannel areas. The varying relative dominance and position of the different parts of the submarine fan system through time resulted in a high degree of lateral and vertical variation. This is represented in the lithologies found in the system and their associated petrophysical parameters.

The structural zonation schemes in each of the fields have been unified and extended out with the field areas (Table 1). The geological model consists of 5 reservoir Zones (E, F, H, J and K), capped by a seal (Zones M and L). The reservoirs overlie a field-wide discontinuity between Zones E and D, so that Zone D is mostly (for Forties) or entirely (for Nelson) under the water-oil-contact. The geological model contains a field-wide permeability barrier between Zones H and J. This barrier is also referred to as Charlie Shale that produces a notable pressure discontinuity over the west and centre of the Forties field but is thin and discontinuous in the east and south-east of the field. In the east over the Nelson Field the barrier forms part of the top seal, therefore the caprock is thicker for Nelson than Forties. Consequently, most of the Forties Field and a small part of the Nelson Field are divided into two pressure units: Zones J and K (upper pressure unit), and Zones E, F and H (lower pressure unit). Other partially extensive barriers (notably between Zones E and F, and between Zones F and H) are modelled by vertical permeability multipliers. As Zone D is mostly or entirely below the water-oil contact lines of both reservoirs, and Zones M and L form a seal for Forties, only Zones K, J, H, E and F are considered in the study since they include the reservoir units.

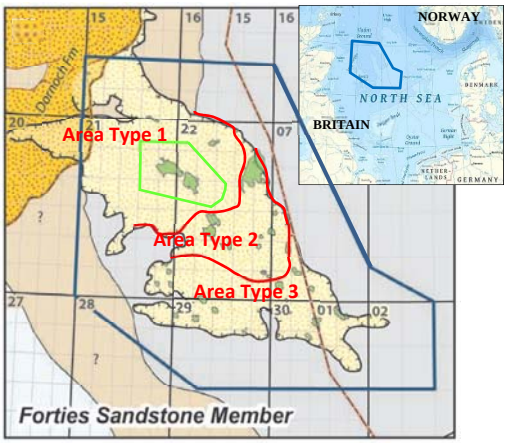

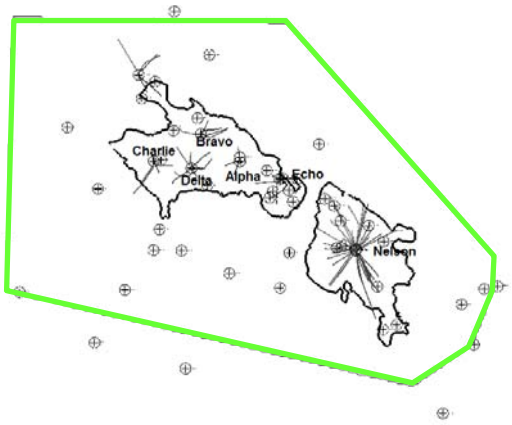

(a) (b)

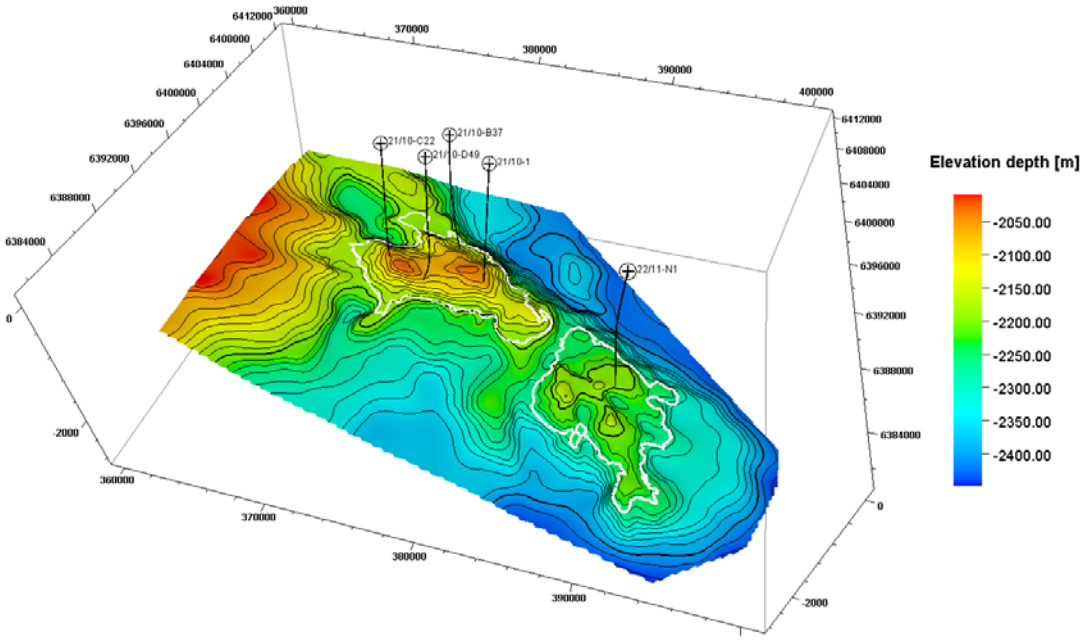

(c)

Figure 1. (a) Central North Sea region showing the distribution of the Forties Sandstone Member, known hydrocarbon accumulations in the member (Robertson et al., 2013), and three Area Types as defined in the Appendix. The study area is shown by a neon green template. (b) The location of the production platforms in Forties: Forties Alpha (FA), Forties Bravo (FB), Forties Charlie (FC), Forties Delta (FD) and auxiliary Forties Echo (FE), and single platform in Nelson. The wells that are scattered across the region have been used for water injection. (c) The elevation map of the top surface of the study area and the wells used for injection in this study namely 21/10-1 at FA, 21/10-B37 at FB, 21/10-C22 at FC, 21/10-D49 at FD, and 21/11-N1 at N. The vertical direction is exaggerated by a factor of 10.

Table 1. Unification of geological model zonation in Forties by Wills (1991) and Nelson by Kunka *et al*. (2003)

Our Model	FORTIES Model of Wills (1991)	NELSON Model of Kunka (2003)	Facies	Average Thickness (meter)
Zone M (caprock of Sele Formation)	Unit M		mudstone	37
Zone L (caprock)	Unit L	Partially present and very thin over Nelson	mudstone	8
Zone K (upper pressure unit)	Unit K	Partially present and very thin over Nelson	thick bedded sandstone and interbedded sandstone and mudstone	14
Zone J (upper pressure unit)	Unit J			44
Field-wide pressure discontinuity (Charlie Shale)				15
Zone H (lower pressure unit)	Unit H	Zone 5	thick bedded sandstone, and interbedded sandstone and mudstone	22
Zone F (lower pressure unit)	Unit F	Zone 4		39
Zone E (lower pressure unit)	Unit E	Zone 3		40
Field-wide pressure discontinuity				25
Zone D (below oil-water contact)	Unit D	Zones 1 & 2	succession of thin bio-turbated sandstones and mud-rich conglomerate	123

The positions of the channels in each zone and the extent of the Forties and Nelson fields that lay inside each of these zones are illustrated in Figure 2. The extent of storage domes is determined from topography and the original oil-water contact of the reservoir.

Figure 2 also shows the regionalisation of the different zones of the model based on whether they are located inside or outside the structure domes. In order to set this up, we used the horizon surfaces of the different zones in the model and the initial water-oil contact planes of the Forties and Nelson reservoirs, located at 2217 m and 2270 m depth respectively.

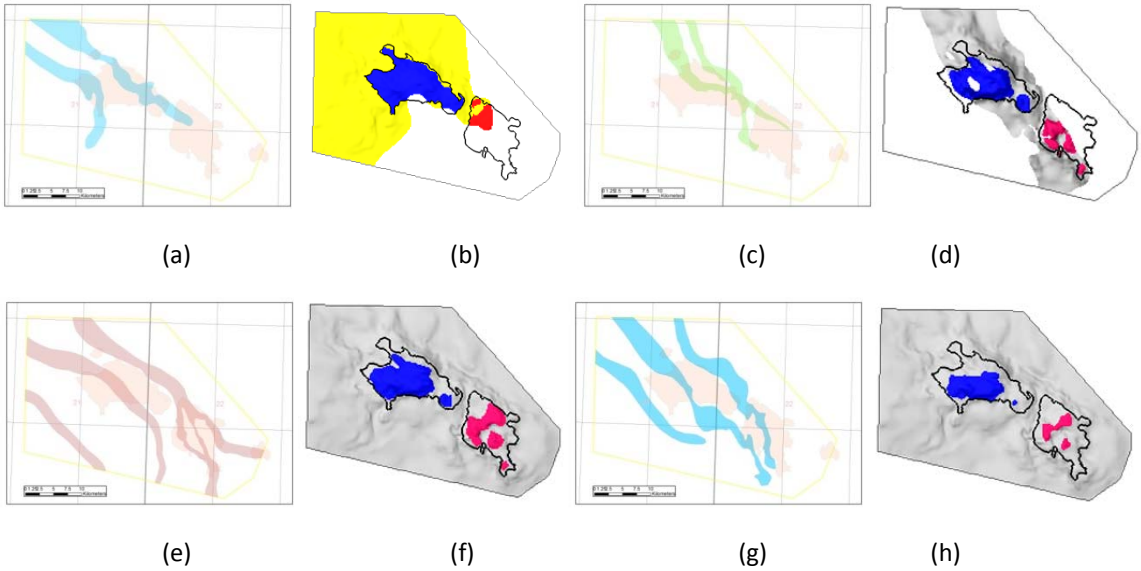

(a) (b) (c) (d)

(e) (f) (g) (h)

Figure 2. (a) The position of channels in **Zones J and K**, (b) regional divisions of Zone J and K, (c) the position of channels in **Zone H** beneath Charlie Shale, (d) regional divisions of Zone H, (e) the position of channels in **Zone F**, (f) regional divisions of Zone F, (g) the position of channels in **Zone E**, (h) regional divisions of Zone E. In (b), (d), (f) and (h) yellow represents part of the Zones J and K that lies outside the Forties and Nelson domes, grey represents part of the Zones E, F and H that lies outside the Forties and Nelson domes, blue the parts that lie within the Forties dome and red the parts that lie within the Nelson dome.

The attribution of the geological model with petrophysical properties, namely porosity, permeability and net-to-gross (NTG) ratio, was carried out using Gaussian random functions. The ranges of values used, including their mean values, are summarised in Table 2 for the different geological facies associations. Some of these values are based on generalisations from the literature such as Kunka *et al*. (2003) and Wills (1991), and in absence of data, average values were assumed by the authors.

Table 2. Petrophysical properties for different facies types from Kunka *et al*. (2003) and Wills (1991) and well log analyses; values indicated as mean (minimum, maximum). For additional information about different facies mentioned in this table please refer to the Appendix.

Petrophysical property	**Channel sands**	**Basal lags (low permeability)**	**Basal lags (high permeability)**	**Shale doggers**	**Interchannel (Slump debris and Mudstones)**	**Slump bodies**
Porosity (%)	25 (21, 38)	25 (21, 38)	25 (21, 38)	< 12	24.6 (3, 32.9)	13 (3, 32.9)
Horizontal Permeability (mD)	376 (31, 1,610)	376 (31, 1,610)	376 (31, 1,610)	< 1	163 (0.01, 1,769)	50 (0.01, 1,769)
Vertical Permeability (Multiplier)	0.1	0.01	0.1	1	0.001-0.01	0.001-0.01
NTG	0.72 (0.21, 1)	0.72 (0.21, 1)	0.72 (0.21, 1)	0.21 (0.21, 1)	0.33 (0.11, 0.89)	0.11 (0.11, 0.89)

A realisation was generated based on the above-mentioned properties at a grid resolution of 100 m × 100 m × 2 m. The profiles of horizontal and vertical permeability, porosity and net-to-gross ratio are shown in Figure 3. The same realisation with the specified resolution is used for flow modelling.

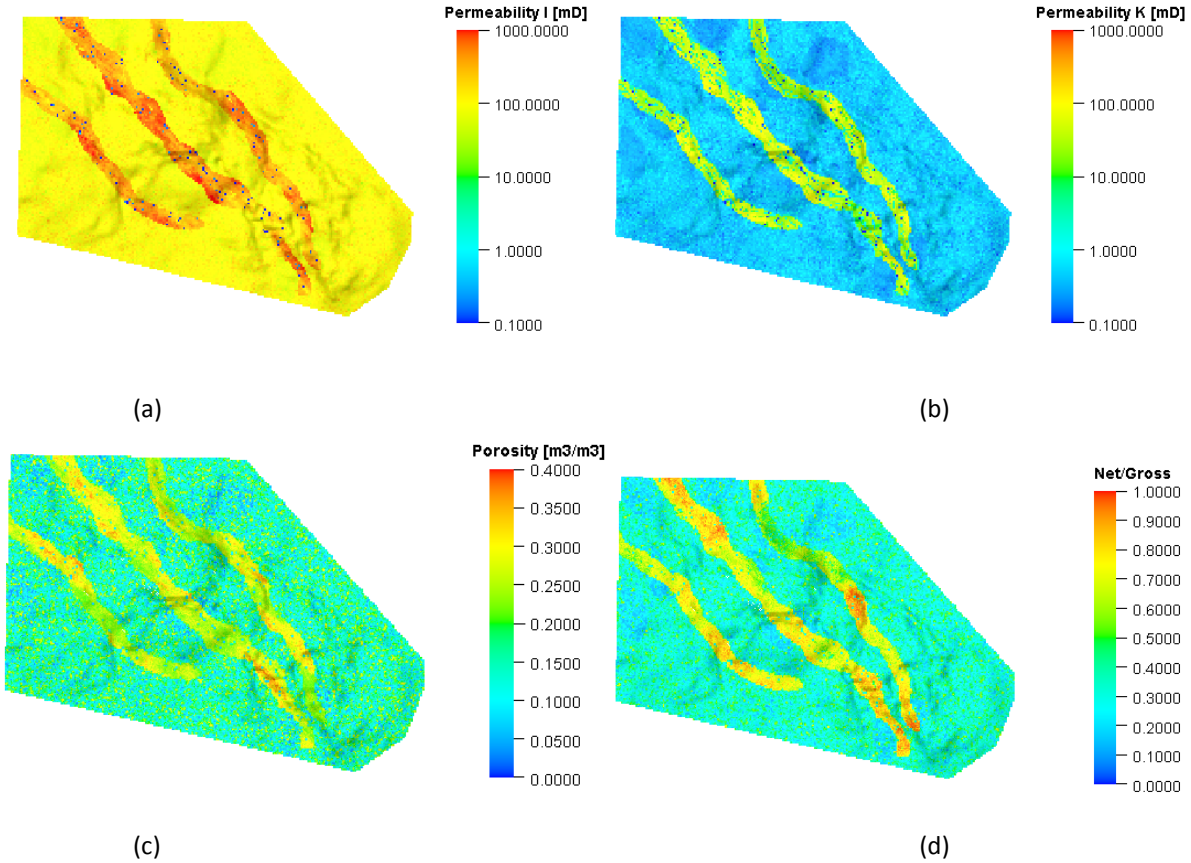

Figure 3. (a) Horizontal permeability (millidarcy), (b) vertical permeability (millidarcy), (c) porosity, and (d) net-to-gross ratio for top of Zone E.

3. Simulation of hydrocarbon production for calibrating the model

In this section the aquifer model is calibrated using historical hydrocarbon production and water injection data from the DECC database (DECC, 2007), as well as the historical pressure data found in the literature. Some of the properties of the hydrocarbon and resident water derived from literature for the two oil fields are summarised in Table 3. The oil-gas and water-gas relative permeability curves are derived from Cawley *et al*. (2005) who studied an enhanced oil recovery using CO_2 at a segment of the Forties Field. It is assumed these curves are applicable for the fluids across the entire domain of the study area in this work.

Table 3. Reservoir fluid properties from Wills (1991), and Kunka *et al*. (2003).

	Forties	**Nelson**
Hydrocarbon		
Initial oil saturation [S_{oi}]	≈0.85	≈0.80
Initial oil in place [V_{oSi}] (standard million m^3 or sm^3)	690	125
Formation volume factor [B_o] (reservoir m^3/standard m^3 or rm^3/sm^3)	1.24–1.32	1.36
Initial oil in place (reservoir million m^3)[V_{oi}= V_{oSi}× B_o]	≈883	170
Dome volume above water-oil contact (reservoir million m^3)[V_{oi}/S_{oi}]	1,038	212
Recovery factor by 2013	0.62	0.58
Formation water		
Salinity (ppm of NaCl)	55,500	84,000
Resistivity (ohm m)	0.034	N/A
Reservoir conditions		
Temperature (°C)	96 at 2175	107 at 2255 m
Initial pressure (bar)	222 at 2175 m	229
Oil-water contact	2217 m	2270 m

In addition to the data above, we assume formation brine has a coefficient of isothermal compressibility of $3.5 \times 10^{-5}\text{bar}^{-1}$ and rock has a coefficient of isothermal compressibility of $4.5 \times 10^{-5}\text{bar}^{-1}$.

An objective of the model calibration is to determine the pore volume multiplier (PVM) that will be used in the simulations to establish the boundary conditions accounting for the pressure support from the surrounding aquifer system. PVM applied on the boundary grid blocks effectively enlarges the domain, which in turn has a direct effect on the pressure behaviour. Obviously, the larger the value of the multiplier, the less the pressure depletion during production will be. In order to establish a reasonable value, the data for pressure decline at start of the production and the pressure build-up at start of the water injection are also used.

According to Brand *et al*. (1996) and Wills (1991), in the first 5 years after production started (by start of 1981), the pressure in the oil bearing sandstone layers of Forties declined by 55-70 bar below the original level. Brand *et al*. (1996) provided pressure depletion profiles in two sandstone regions of Forties (Zones E, F and H in the centre and east and Zones J and K in the west). Permeability restrictions exist between the sand bodies of the field (south-east Forties) that cause significant pressure differences between them (Brand *et al*., 1996).

With the aquifer support having come into effect, coupled with the increasing water injection by 1994, the reservoir pressure rose back to around 14 bar below the original hydrostatic level. Moreover, Simpson and Paige (1991) report that the Forties reservoir pressure was maintained by basal aquifer influx initially, prior to the supplementation of peripheral seawater injection. For the Nelson Field, it is reported by Kunka *et al*. (2003) that by July 1997, 3 years after the production started, the pressure depletion was similar to Forties, around 55-70 bar below the initial level. Here,

225 it is assumed that the pressure drop would be compensated by a combination of the basal aquifer
226 support and peripheral seawater injection over time.

227 Based on the above information and assumptions, the PVM is determined by matching the
228 simulated regional pressures with pressure behaviour of the Forties and Nelson oilfields. The target
229 is a post-production average pressure decline of around 70 bar over the oilfield regions that can be
230 compensated later on during the simulation. The multiplier of PVM = 20 that leads to a reasonable
231 behaviour of the field pressure in the production stage is used for the CO_2 injection simulations. This
232 multiplier applied on the boundary blocks increased the formation pore volume in the whole system
233 from 8,552 million rm^3 to 42,548 million rm^3.

234 The yearly cumulative oil and water production from Forties and Nelson are shown in Figure 4(a) and
235 Figure 4(b). Except for the overestimations of water production at some stages, the graphs show a
236 good agreement between the simulation results and the actual data. The average pressure for areas
237 including Forties and Nelson are shown in Figure 4(c). A post-production pressure decline of up to 70
238 bar is observed that was later compensated for by water injection and water influx from the
239 boundaries. It is noted that the pressure profiles from literature and simulation do not accurately
240 represent the true average pressures from the geological units; however, the trends are in
241 reasonable agreement. Another reason for the observed discrepancy and delayed pressure recovery
242 of our model against the existing data can be probably linked to the insufficiency of considering PVM
243 as the only parameter for model calibration. A PVM > 20 would create pressure profiles with too
244 small reduction during initial years, whereas a PVM < 20 result in pressure profiles with too large
245 reduction during initial years and too little post-water-injection increase. In conclusion, based on a
246 reasonable agreement between data and our model, the assumption will be made that the pressure
247 has been restored to the initial hydrostatic level prior to CO_2 injection.

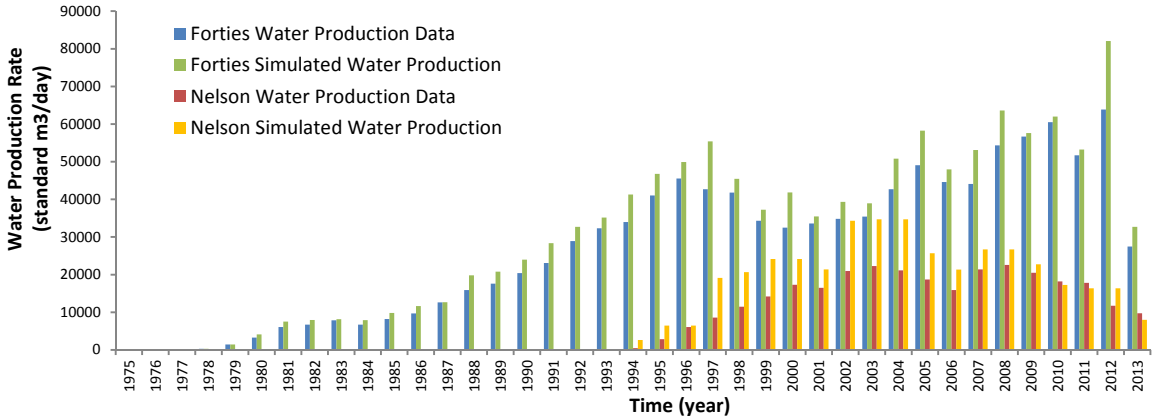

(a)

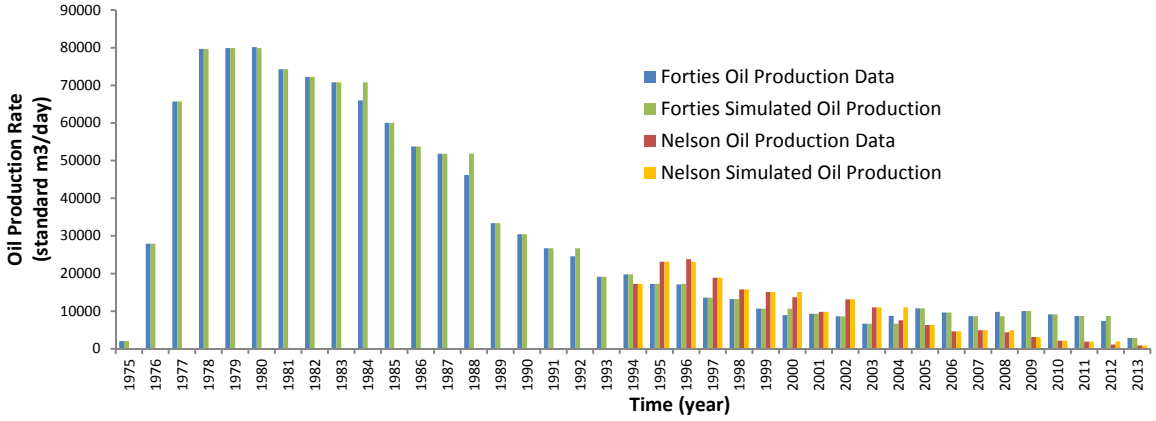

(b)

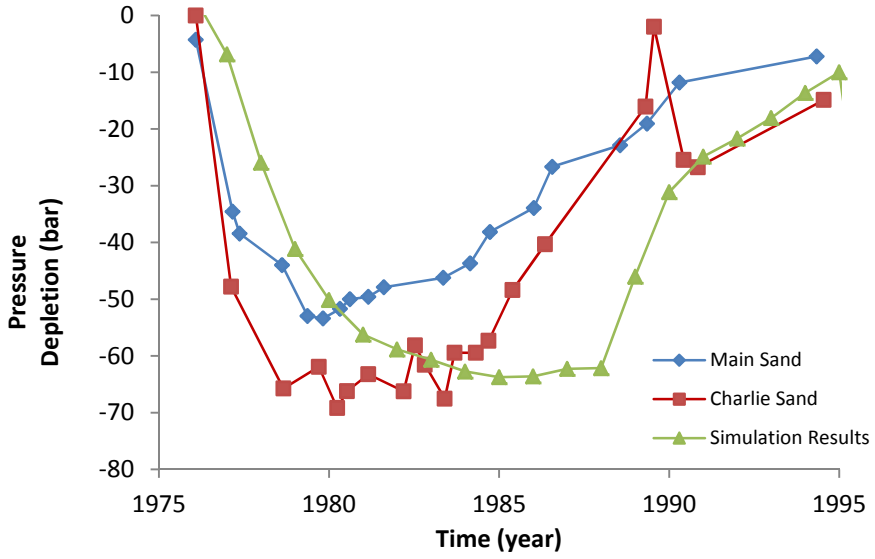

(c)

Figure 4. (a) The yearly oil production rates from the Forties and Nelson oilfields, (b) the yearly water production rates from the Forties and Nelson oilfields, simulation results compared to the actual data from DECC (2013). (c) The pressure depletion profiles from the hydrocarbon production simulation. Also shown are the field data for Charlie Sand (mostly coinciding with Zones J and K) and Main Sand (mostly coinciding with E, F and H) from Brand *et al*. (1996).

4. Dynamic capacity calculation

4.1 Definitions of the key performance indicators (KPIs)

To assess injection scenarios, a number of KPIs are defined and calculated throughout the injection and post-injection periods. These parameters are:

1) Well bottomhole pressure build-up ratio:

$$r_{p,W}^{t} = \frac{p_{bh,W}^{t}}{p_{h,i}^{t_0}} \tag{1}$$

where $p_{bh,W}^{t}$ represents the well bottomhole pressure of a well W at a simulation time t, $p_{h,i}^{t_0}$ represents the hydrostatic pressure at initial time t^0 of the block i in the 100 m × 100 m × 2 m grid. Therefore $r_{p,W}^{t}$ is the ratio of the well bottomhole pressure over the initial hydrostatic pressure of the perforated depth. This measure indicates the local pressure increase of the system due to CO_2 injection and should be limited to some certain values according to the fracture pressure avoidance constraint.

2) Mass fraction of CO_2 in various regions of the domain:

$$x_{m,R}^{t} = \frac{m_{CO_2,R}^{t}}{m_{CO_2}^{t}} \tag{2}$$

where $m_{CO_2,R}^{t}$ represents the mass of CO_2 present in a region R at a simulation time t and $m_{CO_2}^{t}$ represents the total mass of CO_2 injected into the system by simulation time t. Therefore $x_{m,R}^{t}$ is the mass fraction of injected CO_2 in region R at simulation time t.

To help track the CO_2 plume movement and spillage outside the storage dome, the model domain is divided into four control regions:

- the Forties dome: *Region 1*
- the Nelson dome: *Region 2*
- areas lying outside the domes in Zones J and K (Forties upper pressure unit): *Region 3*
- areas lying outside the domes in Zone E, F and H (Forties lower pressure unit): *Region 4*

We define:

$$x_{m,1}^{t} = \frac{m_{\text{gaseous CO2,R1}}^{t} + m_{\text{dissolved CO}_2\text{,R1}}^{t}}{m_{\text{CO}_2}^{t}}$$

$$x_{m,2}^{t} = \frac{m_{\text{gaseous CO2,R2}}^{t} + m_{\text{dissolved CO}_2\text{,R2}}^{t}}{m_{\text{CO}_2}^{t}}$$

$$x_{m,3}^{t} = \frac{m_{\text{gaseous CO}_2\text{,R3}}^{t}}{m_{\text{CO}_2}^{t}}$$

$$x_{m,4}^{t} = \frac{m_{\text{gaseous CO}_2\text{,R4}}^{t}}{m_{\text{CO}_2}^{t}} \tag{3}$$

where $x_{m,1}^{t}$ and $x_{m,2}^{t}$ indicate the level of containment of CO_2 inside the Forties and Nelson structures, and $x_{m,3}^{t}$ and $x_{m,4}^{t}$ indicate the gaseous CO_2 remained outside of the dome structures at time t. Only the gaseous portion of CO_2 is considered in $x_{m,3}^{t}$ and $x_{m,4}^{t}$, because

it is assumed that the dissolved CO_2 implies less risk of leakage to the surface from regions outside the dome structures. Therefore $x_{m,3}^t$ and $x_{m,4}^t$ cannot be used for mass balance calculations, and they are defined as such only for leakage potential. It should be noted that Region 3 lies in Zones J and K (the part of Forties upper pressure unit shown in yellow in Figure 2b), which is penetrated by a large number of abandoned wells. This, together with the fact that Zone J is also in immediate contact with the caprock, makes this region prone to risk of CO_2 leakage through abandoned wells and the caprock outside of the dome. Therefore, reducing $x_{m,3}^t$ must be one objective of the injection design.

3) Fraction of capacity utilised:

$$e_{V,R}^t = \frac{V_{\mathrm{CO}_2,R}^t}{PV_R} \tag{4}$$

where $V_{\mathrm{CO}_2,R}^t$ represents the summation of gaseous and aqueous volumes of CO_2 at reservoir conditions in a region R at a simulation time t and PV_R represents the pore volume of the region R at reservoir conditions. Therefore $e_{V,R}^t$ is the fraction of capacity of the region R utilised at simulation time t. Obviously, the larger this value is, the more efficient the storage operation is. It should be noted that this metric should not be confused by commonly used "storage efficiency" defined by van der Meer (1995) as "the ratio between the maximum storage volume and the actual injected volume." Here this metric is calculated in terms of the volume of CO_2 injected in the section of the reservoir formation that is inside the perimeter of the reservoirs' boundaries rather than the whole aquifer volume and therefore the values will be higher than the storage efficiency values because the denominator is much smaller.

In our model, PV_R for Region 1 is 1,042 million rm^3 (compared to 1,038 million rm^3 in Table 3 for Forties dome), for Region 2, PV_R is 219 million rm^3 (compared to 212 million rm^3 in Table 3 for Nelson dome), for Region 3, PV_R is 4,435 million rm^3 and for Region 4, PV_R is 36,852 million rm^3, note that PVM acts only on the pore volume of the boundary blocks of Regions 3 and 4. The discrepancies between the pore volumes of our model and the actual reservoirs can be attributed to the stratigraphical inaccuracies.

4.2 Definitions of constrained injection scenarios

For calculating the dynamic capacity of the Forties Field and at the same time utilising its storage capacity optimally, four vertical injection wells were located on the main platforms in Forties and one was placed on the Nelson Field platform. The injection pressure is constrained so as not exceed 0.9 multiplied by the fracture pressure of the injection depth:

$$p_{bh,W}^t \le 0.9 \times p_{f,W} \xrightarrow{p_{f,W}=(g_f/g_h)p_{h,i}^{t0},\quad r_{p,W}^t=p_{bh,W}^t/p_{h,i}^{t0}} r_{p,W}^t \le 0.9 \times g_f/g_h \tag{5}$$

where $p_{f,W}$ is the fracture pressure at perforation depth of well W, g_f is the fracture gradient of the system, g_h is the hydrostatic gradient of the system, and $p_{h,i}^{t0}$ is the initial hydrostatic pressure (defined at the centre of the 100 m × 100 m × 2 m gridblock, i) at a reference depth of top of Zone H where bottomhole pressure of well W is also calculated. All the wells are assumed to be 0.3048 metres in diameter, the fracture gradient for the Forties Sandstone Member is assumed 1 psi/ft or 0.226 bar/m (Cawley at al., 2005), and the hydrostatic gradient is assumed 0.54 psi/ft or 0.122 bar/m. Therefore, the pressure constraint is reduced to:

$$r_{p,W}^t \le 1.66 \tag{6}$$

For the five wells of the system, at initial time and at top of Zone H just below the Charlie Shale, we have $p_{h,FA}^{t0} = 248$ bar, $p_{h,FB}^{t0} = 245$ bar, $p_{h,FC}^{t0} = 236$ bar, $p_{h,FD}^{t0} = 245$ bar and $p_{h,N}^{t0} = 241$ bar.

To implement the migration constraint, we define a total target injection rate of Q_{inj}^{total} (million tonnes per annum, hereafter denoted as MTY^{-1}) to be apportioned between five injection wells based on a time varying weight of injectivity index of each well with respect to sum of all wells' injectivity indices, so that:

$$Q_{inj,W}^{t} = \begin{cases} f^{t-1} \times \left(\dfrac{Q_{inj}^{total} \times \left(\sum_{c=1}^{Nc} II_{W,c}^{t-1} \right)}{\sum_{W \epsilon \mathbb{W}1} \left(\sum_{c=1}^{Nc} II_{W,c}^{t-1} \right)} \right) + (1 - f^{t-1}) \times \left(\dfrac{Q_{inj}^{total} \times \left(\sum_{c=1}^{Nc} II_{W,c}^{t-1} \right)}{\sum_{W \epsilon \mathbb{W}2} \left(\sum_{c=1}^{Nc} II_{W,c}^{t-1} \right)} \right), & W \epsilon \mathbb{W}2 \\ f^{t-1} \times \left(\dfrac{Q_{inj}^{total} \times \left(\sum_{c=1}^{Nc} II_{W,c}^{t-1} \right)}{\sum_{W \epsilon \mathbb{W}1} \left(\sum_{c=1}^{Nc} II_{W,c}^{t-1} \right)} \right), & W = FC \end{cases} \tag{7}$$

$$f^{t-1} = \begin{cases} 1, & \left(x_{m,3}^{t-1} \times m_{\mathrm{CO}_2}^{t-1} \right) \leq 0.1 \; million \; tonne \\ 0, & \left(x_{m,3}^{t-1} \times m_{\mathrm{CO}_2}^{t-1} \right) > 0.1 \; million \; tonne \end{cases} \tag{8}$$

where:

- $Q_{inj,W}^{t}$ is the "target" injection rate of well W at time t, actual injection rate can be lower when the bottomhole pressure constraint for the well of interest is violated,
- $II_{W,c}^{t-1}$ is the injectivity index of well W at connection (perforation) c and at time $t-1$, calculated as $II_{W,c}^{t-1} = Q_{inj,W}^{t-1} / (p_{bh,W,c}^{t-1} - P_e^{t-1})$, where $p_{bh,W,c}^{t-1}$ is the bottomhole pressure of well W, at depth of connection c and at time $t-1$, and P_e^{t-1} is the pressure at the vicinity of connection c of well W at time $t-1$,
- N_W and N_c are the number of wells and number of connections for each well,
- $\mathbb{W}1$ is a set of wells including all five injection wells,
- $\mathbb{W}2$ is a set of all wells except for FC,
- f^{t-1} is a multiplier that is 1 when the amount of gaseous CO_2 in Region 3 has not exceeded the threshold of 0.1 million tonne. As soon as this threshold is exceeded, f^{t-1} is set to zero
- $x_{m,3}^{t-1}$ and $m_{\mathrm{CO}_2}^{t-1}$ are as defined previously, the fraction of gaseous CO_2 in Region 3 and the total amount of CO_2 (in moles) of gaseous and aqueous CO_2 in all regions at time $t-1$.

Above formulation apportions, initially, the total amount of available injection gas, to all five wells proportional to their injectivity indices by the vector of $Q_{inj}^{total} \times \left(\sum_{c=1}^{Nc} II_{W,c}^{t-1} \right) / \left(\sum_{W \epsilon \mathbb{W}1} \left(\sum_{c=1}^{Nc} II_{W,c}^{t-1} \right) \right)$. However, since well FC contributes significantly to the migration of CO_2 outside the domes through Region 3 (the risk-prone region), this well is shut off when the migration constraint is violated ($f^{t-1} = 0$) and the total amount of gas is divided between other wells by the vector of $Q_{inj}^{total} \times \left(\sum_{c=1}^{Nc} II_{W,c}^{t-1} \right) / \left(\sum_{W \epsilon \mathbb{W}2} \left(\sum_{c=1}^{Nc} II_{W,c}^{t-1} \right) \right)$. This approach ensures maximum injection of CO_2 into the two dome structures with the specific pressure and migration constraints honoured.

The question in this work can be summarised as:

What is the maximum amount of CO_2 that we can inject (actual cumulative injection denoted by q_{inj}^{cumul}) into the two structures by five available injection wells so that:

- the pressure constraint is not violated at any time;

- a specific threshold of 0.1 million tonne of gaseous CO_2 is the maximum permissible amount that can migrate into the Zones J and K outside the dome structures (Region 3) of the model.

A range of Q_{inj}^{total} is prescribed in a 30-year injection period. The simulations are continued for a 50-year post injection monitoring period to record KPIs. The simulations are conducted on a HP ProLiant Server with 12-core processor, allowing parallel simulations at the time with Schlumberger's ECLIPSE E300 compositional simulator with CO2STORE option for CO_2 storage in saline aquifers. Each simulation takes about 17,849 seconds on the server.

5. Results

In order to find the pressure and migration constrained injection strategy, we conduct 20 simulations of Q_{inj}^{total} ranging from 1 to 20 MTY^{-1}. The actual total injected CO_2 (q_{inj}^{cumul}) is shown in Figure 5(a) for increasing Q_{inj}^{total}. It is observed that when Q_{inj}^{total}= 12 MTY^{-1}, the pressure constraint has led to $q_{inj}^{cumul} < \left(30 \text{ years} \times Q_{inj}^{total}\right)$, thereby actual injected gas is less than the target injection. Figure 5(b) shows the maximum amount of spilled gaseous and dissolved CO_2 in Region 3 and 4 or $x_{m,R}^{t=30 \text{ years}} \times m_{CO_2}^{t=30 \text{ years}}$ in million tonnes. For this figure, Q_{inj}^{total}= 8 MTY^{-1} is a threshold injection rate above which the specifically defined threshold of 0.1 million tonnes CO_2 in Region 3 is violated. This is despite the fact that the injection strategy switches off the injection at FC to prevent the migration constraint being violated. In other words FA, FB and FD (only FB as will be shown later) are contributing to the migration for Q_{inj}^{total}> 8 MTY^{-1}. In Figure 5(b), we also showed the dissolved CO_2 versus Q_{inj}^{total} for Region 3 and Region 4 by end of the injection period.

Figure 5(c) shows the total actual injected gas for each well per Q_{inj}^{total}. The injectivity-index-based apportioning of rate chooses FC as the most suitable injection location between all five wells, and after FC is shut early in the simulation (for Q_{inj}^{total}= 4 MTY^{-1} and higher), N becomes the most suitable location. Then at Q_{inj}^{total}= 12 MTY^{-1} and higher, N initially gets higher proportions of injection, but because Q_{inj}^{total} is high, N violates the pressure constraint (Figure 5d) and therefore its injection rate is reduced so that by Q_{inj}^{total}= 16 MTY^{-1}, FB becomes the well with the highest cumulative gas injection of the system, despite the fact that FB itself reaches to the threshold of $r_{p,W}^{t} = 1.66$ sometime in the simulation. For all the simulations, $r_{p,W}^{t}$ at 30 years for each well and for each Q_{inj}^{total} is shown in Figure 5(d).

In our 3D model, FA and FD have relatively low injectivity indices and therefore they are not favourable for injection. The low injectivity is also manifested for high Q_{inj}^{total} where even small proportions of injection gas lead to FA and FD reaching $r_{p,W}^{t} = 1.66$ during the simulation (Figure 5d). A favourable location of FC (next to the Forties spill point to Zones J and K), and then FB which is located away from the spill point to Zones J and K and away from abrupt discontinuity of Zones J and K towards the east outweigh the injectivity of FA and FD.

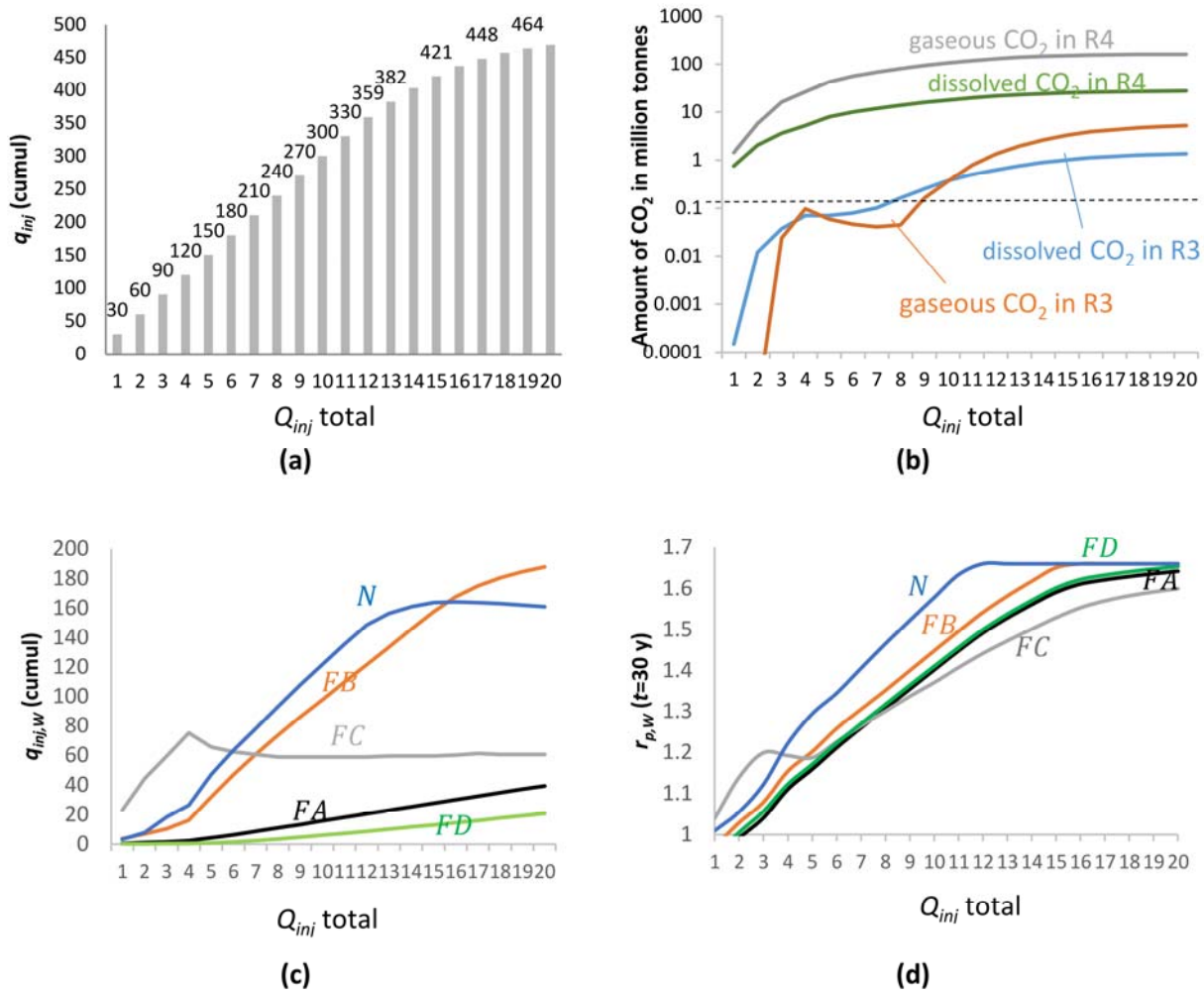

Figure 5. (a) Cumulative (actual) gas injected versus $\boldsymbol{Q_{inj}^{total}}$, (b) the amount of CO_2 in gaseous phase in Region 3 versus $\boldsymbol{Q_{inj}^{total}}$, (c) Cumulative (actual) gas injected for each well versus $\boldsymbol{Q_{inj}^{total}}$, and (d) the ratio of pressure increase at year 30 for each well versus $\boldsymbol{Q_{inj}^{total}}$.

Figure 6 shows the profiles of gaseous CO_2 ($x_{m,R}^{t=30\ years} \times m_{CO_2}^{t=30\ years}$) and fraction of capacity utilised by increase in Q_{inj}^{total}. For Nelson we reach plateaus for both quantities at Q_{inj}^{total}= 14 MTY^{-1}. Therefore increase in Q_{inj}^{total} does not necessarily lead to increase in fraction of capacity utilised. Figure 6(a) shows that Forties dome is capable of accommodating around 121 million tonnes of CO_2 applying the selected injection rate of Q_{inj}^{total}= 8 MTY^{-1} (corresponding to a total amount of injection of 240 million tonnes). For Nelson the value is 24 million tonnes. Therefore, based on our migration constraint of less than 0.1 million tonnes of gaseous CO_2 in Region 3 (the pressure constraint is not limiting injection for Q_{inj}^{total}= 8 MTY^{-1}), the dynamic capacities of Forties and Nelson stand at 121 million tonnes and 24 million tonnes respectively. Corresponding fraction of capacity utilised for Forties and Nelson are shown in Figure 6(b), where at Q_{inj}^{total}= 8 MTY^{-1}, both $e_{V,R1}^{t=30\ \text{years}}$ and $e_{V,R2}^{t=30\ \text{years}}$ curves intersect each other at 0.147.

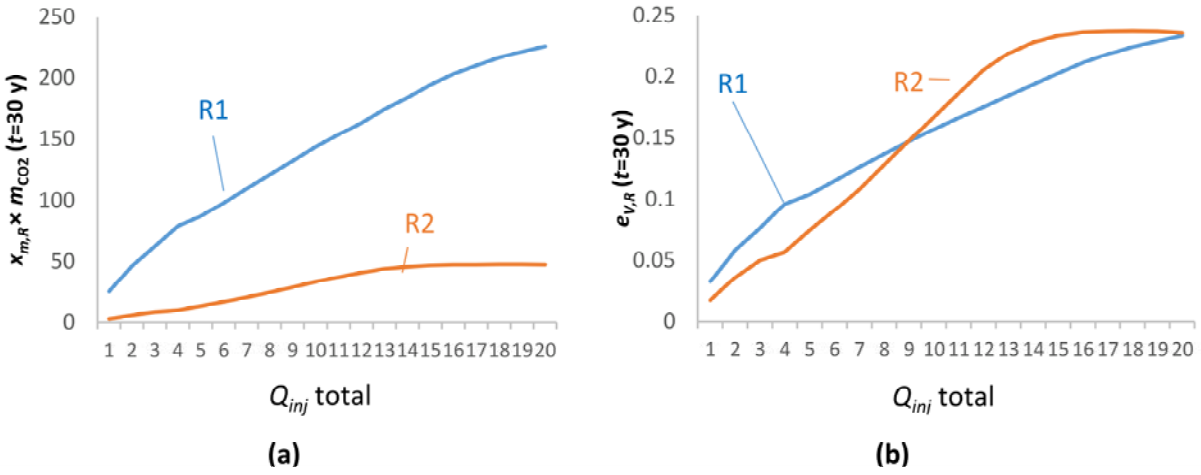

Figure 6. (a) The amount of CO_2 in gaseous phase at Regions 1 and 2 versus Q_{inj}^{total}, and (b) the volumetric storage efficiency for Regions 1 and 2 (Forties and Nelson dome structures, respectively) at year 30 versus Q_{inj}^{total}.

To visualise the distribution of CO_2 in the 3D model, for monitoring purposes we additionally simulate a 200 year post-injection period using Q_{inj}^{total}= 8 MTY^{-1} and its corresponding injection strategy with the well injection rates shown in Figure 7(a) and resultant bottomhole pressure profiles in Figure 7(b) for the 30-year injection period.

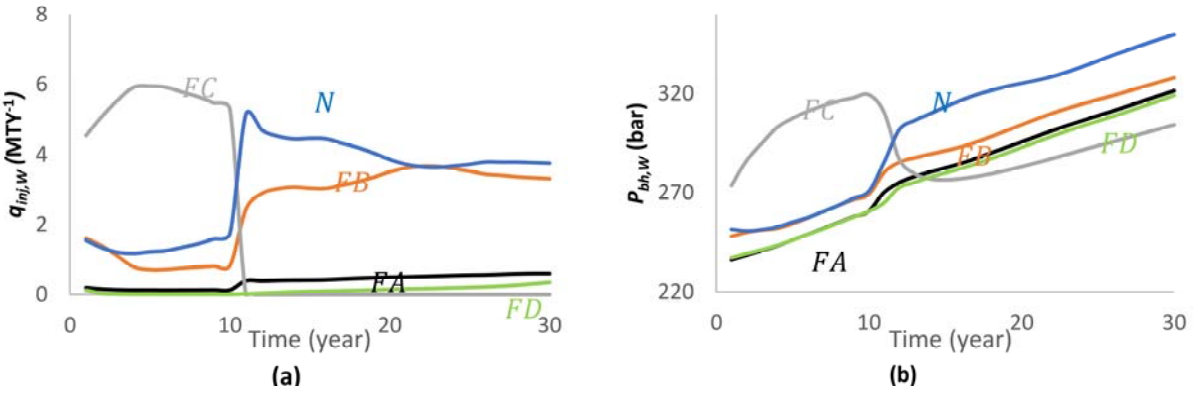

Figure 7. (a) The dynamically varying injection rates for the five injection wells corresponding to Q_{inj}^{total}= 8 MTY^{-1} for the 30-year injection period. FC is shut for year 10 because of the migration constraint. (b) $P_{bh,W}^{t}$ for the five injection wells corresponding to Q_{inj}^{total}= 8 MTY^{-1} for the 30-year injection period. None of the wells are affected by the pressure constraint at this Q_{inj}^{total}

Figure 8(a) shows the spread of CO_2 gas saturation after 230 years of simulation for all regions of the 3D model. We filtered out the blocks that have less than 0.01 gas saturation. Figure 8(b) shows the extent of gaseous CO_2 (S_g > 0.01) outside the dome structures in Region 3 only. Clearly there is only a negligible amount of gas in Region 3. Figure 8(c) shows the extent of gaseous CO_2 (S_g > 0.01) outside the dome structures in Region 4 only. Underneath the Nelson dome, a significant amount of gas has been stored, because the Nelson well, N, has been on operation with a high injection rate after well FC is shut.

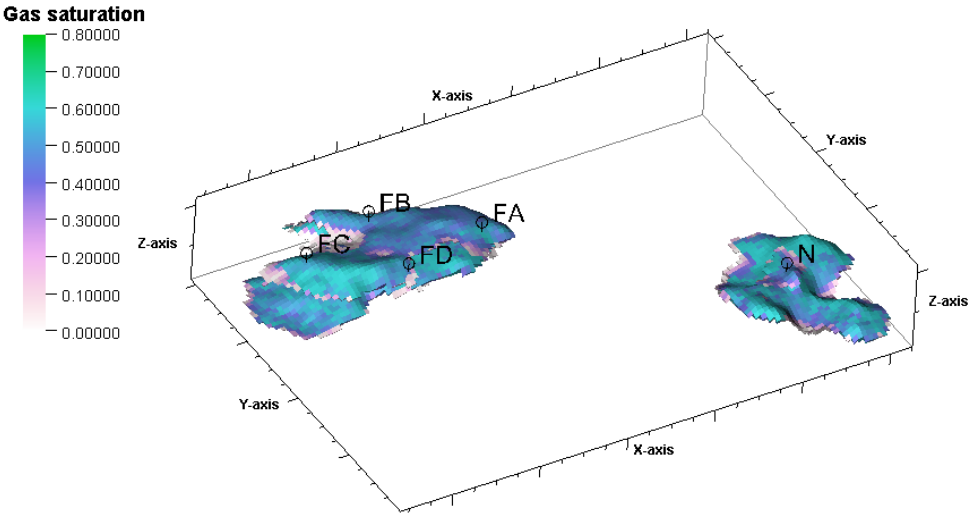

440
441

(a)

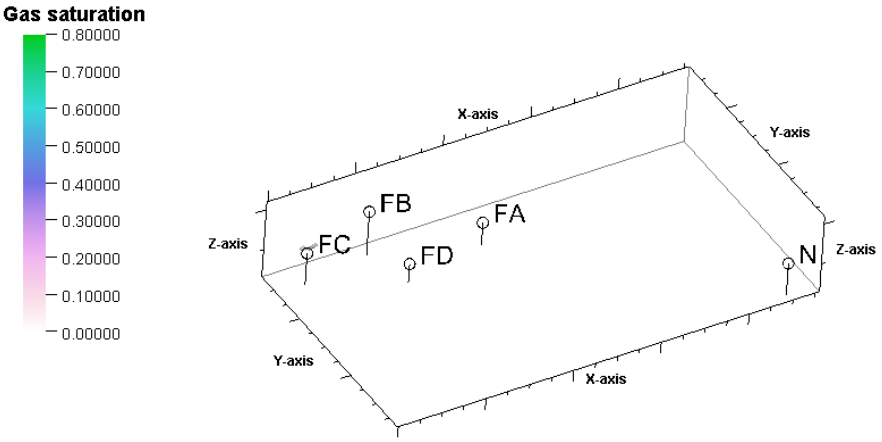

442
443

(b)

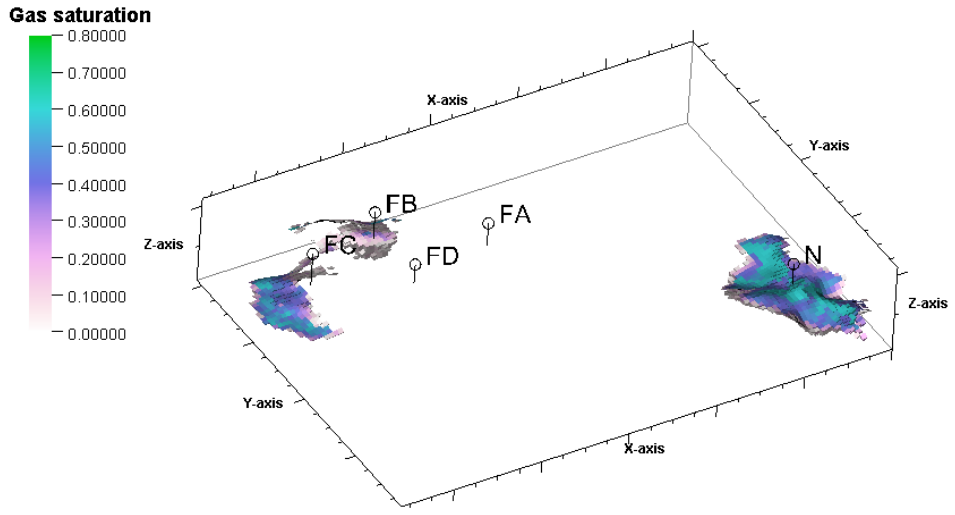

444
445

(c)

446 **Figure 8**. The gas saturation (S_g) distribution 200 years after CO_2 injection stopped. (a) The distribution for all
447 blocks with $S_g > 0.01$, (b) the distribution for blocks belonging to Region 3 only with $S_g > 0.01$, and (c)
448 the distribution for blocks belonging to Region 4 only with $S_g > 0.01$.

6. Conclusions and future work

The authors have constructed a detailed geological model that encompasses the Forties and Nelson dome structures and the surrounding aquifer system located in the UK Central North Sea. Historical data for hydrocarbon production was used to calibrate the model in terms of the aquifer support for pressure by scaling the pore volumes at the boundaries of the model. A number of key performance indicators for CO_2 storage including the ratio of pressure increase, regional mass fractions, and fraction of capacity utilised alongside the injection strategy constrained by both pressure and migration were defined. It was assumed that the structures are fully saturated with brine and consequently our simulations are based on CO_2 storage in saline aquifers.

The injection simulation results for a range of input total injection target rates were used to extract the dynamically varying injection rates weighted by the injectivity indices of the wells. The injection scenarios also honoured the pressure and migration constraints for five wells belonging to the five platforms of the two structures. It was shown that, based on the specific threshold of well bottomhole pressures to stay below 1.66 times the initial hydrostatic pressure, and the migration constraint of having less than 0.1 million tonnes of gaseous CO_2 in Zones J and K outside the dome structures, 121 and 24 million tonnes of CO_2 can be stored in the Forties and Nelson dome structures, respectively. This was achieved by injecting 8 million tonnes of CO_2 per year into the two structures for 30 years. According to the simulation results, 80 million tonnes of CO_2 from the total 240 million tonnes is also expected to migrate in gas phase outside the regions below the Charlie Shale (which we assume it bears less risk of leakage to the surface in comparison with the region above field-wide Charlie Shale).

The calculated total capacity of 145 MT CO_2 corresponds to a total reservoir gas volume of 225 million rm^3 combined from both structures extracted from the simulator outputs[†]. Considering that the original pore volume of the whole domain before application of PVM is 8,552 million rm^3, the storage efficiency is 0.026 or 2.6%. This value agrees with the range of regional-scale storage efficiency values calculated to be 2% by Obi and Blunt, (2006), 2.3% by (Smith *et al*. 2011) and 3.5% by Goater *et al*. (2013) for UK Forties formation, and assumed to be 2% for Dutch CO_2 storage candidate sites by Wildenborg *et al.*, (1998), Damen *et al.*, (2009), and Ramírez *et al.* (2010) and in the range of 0.2% - 2% by SCCS (2009) for the UK North Sea formations. We conclude that in our study a combination of detailed geological data assimilation, dome stratigraphical volume calculation (using the zones' horizons and water-oil contact), and constraining the simulations by pressure and migration, have resulted in reliable storage capacity estimates for Forties and Nelson dome structures.

Future work includes:

- Considering a three phase CO_2-oil-brine system that accounts for oil remaining unproduced from the hydrocarbon production stage. In this way, the feasibility and potentials of CO_2-EOR (Enhanced Oil Recovery) can be assessed and consequently a more realistic situation in which the reservoirs are not assumed fully depleted can be considered.
- Accounting for the uncertainties in the petrophysical properties of the geological model.

[†] This value can also be obtained by assuming a reservoir condition density of CO_2=600 $kg.m^{-3}$, 145 million tonnes / 600 600 $kg.m^{-3}$ = 241 million m^3

Acknowledgements

The authors appreciate the constructive comments of the anonymous reviewers of the paper. This research was carried out as part of the UK Research Councils' Energy Programme funded consortium projects "Multiscale Whole Systems Modelling and Analysis for CO_2 Capture, Transport and Storage", Grant Reference: NE/H01392X/1 and "CO_2 Injection and Storage - Short and Long-term Behaviour at Different Spatial Scales", Grant Reference: EP/K035967/1. The computational resources were provided by the University of Manchester EPS funding. The authors would like to thank this institution.

Appendix – Area-Type definition for *Forties Sandstone Member*

The Forties Sandstone Member comprises submarine fan sandstones made up of a huge number of interconnected amalgamated channels and interchannel areas that change laterally and vertically creating a very complex 'plumbing system'. The 'Forties Fan' can be regarded as an open system - though it is probably closed on its south-eastern, south western and north-eastern sides. It is probably open to the northwest.

The Forties fan is 300 km by 100 km at its widest spread and trends NW-SE and, in general, to the SE the reservoirs will become deeper, and thinner, will have lower mean NTG and lower, but still fair to good, porosities, will have poorer permeabilities (by factor of 10 less). In addition, to the SE, any structural closures present are more likely to be formed by salt movement.

Numerous hydrocarbon fields are located in different parts of the Forties fan:

- **Proximal:** mostly channelised turbidite reservoirs such as Forties and Nelson fields, high NTG (65%), porosity 23-26%, permeabilities hundreds of mD
- **Distal**: turbidite reservoirs less frequently channelised such as Pierce and Starling fields, more typically overlapping lobes and/or sheets, lower NTG (50%), porosity 16-23%, permeabilities tens of mD

There is a clear and progressive downdip thinning: 259 m at the Forties Field (proximal area) and 137 m at the Pierce Field (distal area). Three potential *Area Types* have been identified based primarily on palaeogeography (*i.e.*, location on fan complex) (Figure 1 in the manuscript).

Area Type 1

The 3D model has been built from an area that includes the Forties and Nelson fields located in the central part of the Forties fan. The reservoir in this 3D model exhibits lateral and vertical variation in petrophysical parameters, reflecting the evolution of the Forties submarine fan in a relatively proximal location. The model has been attributed using data from the Forties and Nelson oil fields and information from wells drilled in the area. Each zone in the model is divided into two facies associations namely 'channel' and 'interchannel' areas:

Amalgamated channels

There are four elements to the amalgamated channels – channel sands, low permeability basal lags, high permeability basal lags and intra channel doggers as shown in Figure A1.

Interchannel areas

The 'Interchannel' areas and associated channel margins contain muddy debris flows, slump deposits, thin-bedded turbidites and mudstones. Mudstones form vertical permeability barriers to the sandstones present.

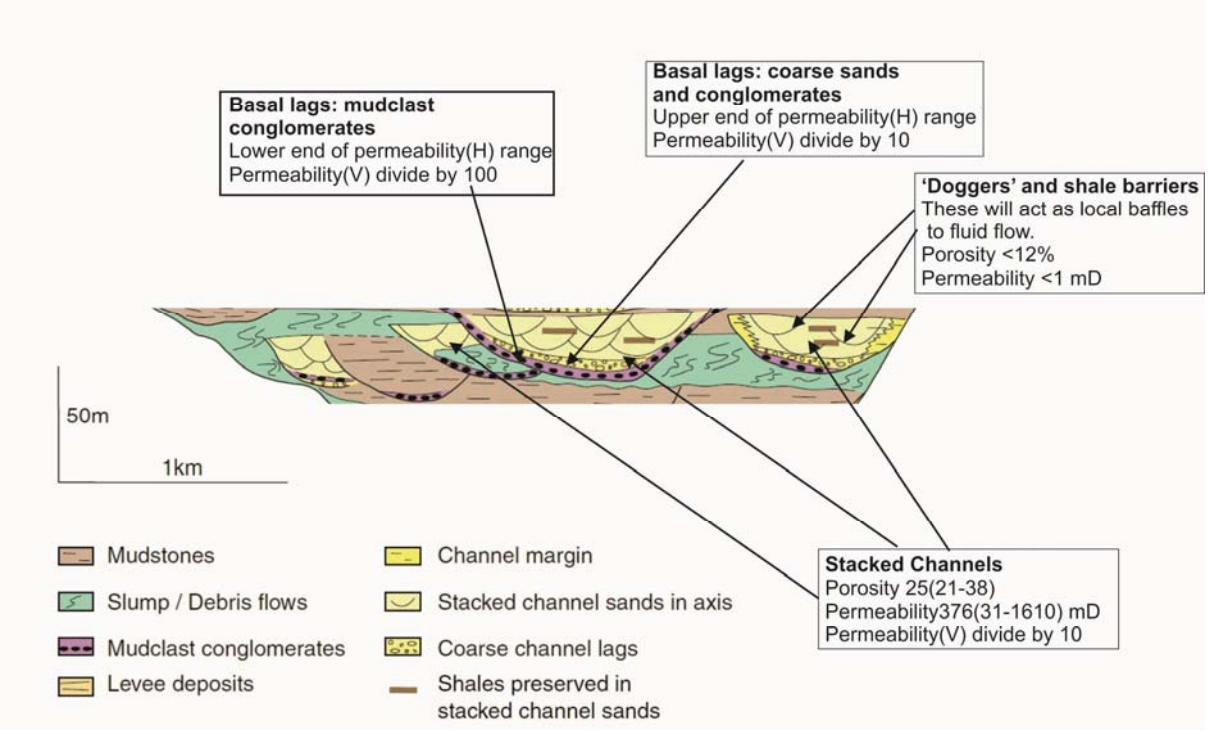

Figure A1. Illustration of different facies in Area Type 1. Cartoon modified after Mayall et al. (2006)

Table 2 in manuscript reports the facies-dependent attributes of the Area Type 1 geological model, and Babaei *et al*. (2016, Tables 1 and 2) summarises the objects' shapes and geometrical parameters used for representing the different facies in Area Type 1**.**

Area Type 2

Area Type 2 reservoir attribution is based on data from Montrose, Arbroath, Arkwright and South Everest fields and core measurements from two wells. The following table reports the data for Area Type 2.

Table A1 – Data for Area Type 2

Data source	Depth to top	Thickness	Porosity	Permeability	NTG
Arbroath & Montrose fields (Crawford et al., 1991; Hogg 2003)	2447.5 & 2451 m	100.6(79.2 – 134.1)	24(3-30)	80(1-2000) Commonly 70 to 90 mD	0.5(0.3 – 0.8)
Arkwright (Kantorowicz 1999)	2578 m	153 m	19.25(15.9 – 21.0)	38.4(24-78)	0.78(0.61 – 0.91)
South Everest (Thompson & Butcher 1991)	2591		21	46	0.67

Well 22/18- 5			22.5(1.5-29)	53.8(0.001-177)	
Well 22/23a- 3			20.44(2.4-28.6)	78.8(0.01-202) Reservoir sands 39(0.01-202) All values	
SUMMARY	2517 m		22(16-30)	80(1-1250)	0.61(0.3-0.91)

Area Type 3

Structures and closures are compact, generally circular, and smaller. The structures are often due to underlying salt movement. Radial faults may act as baffles but unlikely to compartmentalise reservoirs (Birch and Haynes, 2003; Kantorowicz et al., 1999). The following table reports the data for Area Type 3.

Table A2 – Data for Area Type 3

Data source	**Depth to top**	**Thickness**	**Porosity**	**Permeability**	**NTG**
Pierce		145.8 m	18(16-20)	19(1-40)	0.47(0.01-0.77)
Mungo		100 – 400 m	19 -24	10-50	0.43-0.63 to 0.25
Machar			21 average	5-50	
North Everest (Thompson & Butcher 1991)	2560		19	16	0.55
Well 23/22a- 3			17(2.2-22.5)	11.5(0.01-70)	
Well 29/03a- 7		141.7 m	22(2.3-27.1)	297(0.004-675)	
SUMMARY			20(16-27)	20(1-600)	0.51(0.01-0.77)

References

Babaei, M., I. Pan, A. Korre, J.-Q. Shi, R. Govindan, S. Durucan and M. Quinn (2016), CO_2 storage well rate optimisation in the Forties sandstone of the Forties and Nelson reservoirs using evolutionary algorithms and upscaled geological models, *International Journal of Greenhouse Gas Control 50,* 1–13.

Bachu, S. (2015), Review of CO_2 storage efficiency in deep saline aquifers, *International Journal of Greenhouse Gas Control 40,* 188–202.

Birch, P., and J. Haynes (2003), The Pierce Field, Blocks 23/22a, 23/27, UK North Sea. In: Gluyas, J.G. & Hitchens, H.M. (eds). United Kingdom Oil and Gas Fields, Commemorative Millennium Volume. Geological Society, London, Memoir, 20, pp. 647-659.

Birkholzer, J.T., C.M. Oldenberg, and Q. Zhou (2015), CO2 migration and pressure evolution in deep saline aquifers, *International Journal of Greenhouse Gas Control 40,* 203–220.

Brand, P., P. Clyne, F. Kirkwood, and P. Williams (1996), The Forties Field-20 Years Young, *Journal of Petroleum Technology*, *48*(4), 280–291.

Burton, M.M., N. Kumar, S.L. and Bryant (2008), Time-dependent injectivity during CO_2 storage in aquifers, in the 2008 SPE/DOE Improved Oil Recovery Symposium held in Tulsa, Oklahoma, U.S.A., 19–23 April 2008.

Cawley, S.J., M.R. Saunders, Y. Le Gallo, B. Carpentier, S. Holloway, G.A. Kirby, T. Bennison, L. Wickens, and R. Wikramaratna, T. Bidstrup, S.L.B. Arkley and M.A.E. Browne, and J.M. Ketzer (2005), *The NGCAS Project-Assessing the potential for EOR and* CO_2 *storage at the Forties Oil field, Offshore UK-Results from the* CO_2 *Capture Project, v. 2: Geologic Storage of Carbon Dioxide with Monitoring and Verification, SM Benson*, Elsevier Science, London.

Crawford, R., R.W. Littlefair, and L.G. Affleck (1991), The Arbroath and Montrose Fields, Blocks 22/17, 18, UK North Sea. In: Abbotts, I.L. (ed). United Kingdom Oil and Gas Fields, 25 Years Commemorative Volume. Geological Society Memoir No. 14, pp. 211-217.

Damen, K., A. Faaij, W. Turkenburg (2009), Pathways towards large-scale implementation of CO_2 capture and storage: A case study for the Netherlands, *International Journal of Greenhouse Gas Control*, 3(2), pp 217-236

DECC (2007), Well Production Data, Department for Business, Enterprise and Regulatory Reform, [online] Available from: https://www.og.decc.gov.uk/information/wells/pprs/welldataindex.htm

DECC (2013), UK Monthly Oil Production Data, Department of Energy and Climate Change, [online] Available from: https://www.og.decc.gov.uk/pprs/full_production.htm

Doughty, C. and K. Pruess (2004), Modeling Supercritical Carbon Dioxide Injection in Heterogeneous Porous Media, *Vadose Zone Journal* 3 (3). Soil Science Society: 837–47.

Ennis-King, J. and L. Paterson (2005), Role of Convective Mixing in the Long-Term Storage of Carbon Dioxide in Deep Saline Formations, *SPE Journal* 10 (3), Society of Petroleum Engineers: 349–56.

Espie, A. (2001), Options for establishing a North Sea geological storage hub, in *Greenhouse Gas Control Technologies: Proceedings of the Fifth International Conference on Greenhouse Gas Control Technologies, CSIRO Publishing, Collingwood, Victoria, Australia*, pp. 266–271.

Flett, M., R. Gurton, and G. Weir (2007), Heterogeneous Saline Formations for Carbon Dioxide Disposal: Impact of Varying Heterogeneity on Containment and Trapping, *Journal of Petroleum Science and Engineering* 57 (1). Elsevier: 106–18.

Frailey, S. M. (2009), Methods for Estimating CO_2 Storage in Saline Reservoirs, *Energy Procedia* 1 (1). Elsevier: 2769–76.

Goater, A.L., B. Bijeljic and M.J. Blunt (2013), Dipping open aquifers—The effect of top-surface topography and heterogeneity on CO 2 storage efficiency, *International Journal of Greenhouse Gas, 17,* pp. 318-331.

Hempton, M., J. Marshall, S. Sadler, N. Hogg, R. Charles, and C. Harvey (2005), Turbidite reservoirs of the Sele Formation, Central North Sea: geological challenges for improving production, in *Geological Society, London, Petroleum Geology Conference series*, vol. 6, pp. 449–459.

598 Hogg, A.J.C. (2003), The Montrose, Arbroath and Arkwright Fields, Blocks 22/17, 22/18, 22/23a, UK
599 North Sea. In: Gluyas, J.G. & Hitchens, H.M. (eds). United Kingdom Oil and Gas Fields,
600 Commemorative Millennium Volume. Geological Society, London, Memoir, 20, pp. 611-616.
601 Holt, T., J.-I. Jensen, and E. Lindeberg (1995), Underground storage of CO_2 in aquifers and oil
602 reservoirs, *Energy Conversion and Management*, *36*(6), 535–538.
603 Hughes, D., D. Teeuw, C. Cottrell, and J. Tollas (1990), Appraisal of the Use of Polymer Injection To
604 Suppress Aquifer Influx and To Improve Volumetric Sweep in a Viscous Oil Reservoir, *SPE*
605 *Reservoir Engineering*, *5*(1), 33–40.
606 IPCC (2005) Intergovernmental Panel on Climate Change: Special Report on Carbon Dioxide Capture
607 and Storage, (ed.) Metz, B. and Davidson, O. and de Cornick, H. and Loos, M. and Meyer, L.,
608 Prepared by Working Group III of the Intergovernmental Panel on Climate Change Published for
609 the Intergovernmental Panel on Climate Change
610 Kantorowicz, J. D., I.J. Andrews, S. Dhanani, M. Gillis, C. Jennings, P.J. Lumsden, G. Orr, R.W. Simm,
611 and J. Williams (1999), Innovation and risk management in a small subsea-tieback: Arkwright
612 Field, Central North Sea, UK. In: Fleet, A. J. & Boldy, S. A. R. (eds) Petroleum Geology of Northwest
613 Europe: Proceedings of the 5th Conference, 1125-1134. Petroleum Geology '86 Ltd. Published by
614 the Geological Society, London.
615 Ketzer, J.M., B. Carpentier, Y. Le Gallo, and P. Le Thiez (2005), Geological sequestration of CO_2 in
616 mature hydrocarbon fields. Basin and reservoir numerical modelling of the Forties Field, North
617 Sea, *Oil & gas science and technology*, *60*(2), 259–273.
618 Kulpecz, A. A., and L. C. van Geuns (1990), Geological Modeling of a Turbidite Reservoir, Forties Field,
619 North Sea, in *Sandstone Petroleum Reservoirs*, edited by Barwis, John H. and McPherson, John G.
620 and Studlick, Joseph R.J., pp. 489–507, Springer New York.
621 Kumar, A., M. Noh, G.A. Pope, K. Sepehrnoori, S. Bryant, and L.W. Lake (2004), Reservoir Simulation
622 of CO_2 Storage in Deep Saline Aquifers. In *SPE/DOE Symposium on Improved Oil Recovery*.
623 Kunka, J., G. Williams, B. Cullen, J. Boyd-Gorst, G. Dyer, J. Garnham, A. Warnock, J. Wardell, A. Davis,
624 and P. Lynes (2003), The Nelson Field, Blocks 22/11, 22/61, 22/7, 22/12a, UK North Sea,
625 *Geological Society, London, Memoirs*, *20*(1), 617–646.
626 Liao, C., X. Liao, X. Zhao, H. Ding, X. Liu, Y. Liu, J. Chen, and N. Lu (2014), Comparison of Different
627 Methods for Determining Key Parameters Affecting CO_2 Storage Capacity in Oil Reservoirs .
628 *International Journal of Greenhouse Gas Control* 28 (0): 25 – 34.
629 Mathias, S. A., P. E. Hardisty, M. R. Trudell, and R. W. Zimmerman (2009), Approximate Solutions for
630 Pressure Buildup during CO_2 Injection in Brine Aquifers. *Transport in Porous Media* 79 (2).
631 Springer: 265–84.
632 Mayall, M., E. Jones, and M. Casey (2006). Turbidite channel reservoirs – Key elements in facies
633 prediction and effective development. *Marine and Petroleum Geology*, Vol. **23**, pp.821-841.
634 van der Meer, L.G.H. (1995), The CO_2 Storage Efficiency of Aquifers. *Energy Conversion and*
635 *Management* 36 (6). Elsevier: 513–18.
636 van der Meer, L.G.H., and P.J.P. Egberts (2008), A general method for calculating subsurface storage
637 capacity, OTC Paper 19309.
638 van der Meer, L.G.H. and F. Yavuz (2009), CO_2 storage capacity calculations for the Dutch subsurface,
639 *Energy Procedia* 1: 2615–2622.
640 Obi, E. O. I., and M.J. Blunt (2006), Streamline-based simulation of carbon dioxide storage in a North
641 Sea aquifer, *Water Resources Research*, 42(3).
642 Ozah, R.C., S. Lakshminarasimhan, G.A. Pope, K. Sepehrnoori, and S. L. Bryant (2005), Numerical
643 Simulation of the Storage of Pure CO_2 and CO_2-H2S Gas Mixtures in Deep Saline Aquifers. In *SPE*
644 *Annual Technical Conference and Exhibition*.
645 Ramírez, A., S. Hagedoorn, L. Kramers, T. Wildenborg, and C. Hendriks (2010), Screening CO_2 storage
646 options in The Netherlands, *International Journal of Greenhouse Gas Control*, 4(2).

Robertson, J., N.R. Goulty, and R.E. Swarbrick (2013), Overpressure distributions in Palaeogene reservoirs of the UK Central North Sea and implications for lateral and vertical fluid flow, *Petroleum Geoscience*, *19*, Geological Society of London, pp. 223-236.

SCCS (2009), Opportunities for CO_2 Storage around Scotland — an integrated strategic research study, [online] Available from: http://carbcap.geos.ed.ac.uk/website/publications/regionalstudy/CO_2-JointStudy-Full.pdf

Simpson, A., and R. Paige (1991), Advances in Forties field water injection, *Offshore Europe*.

Smith, D.J., D.J. Noy, S. Holloway and R.A. Chadwick (2011), The impact of boundary conditions on CO_2 storage capacity estimation in aquifers, *Energy Procedia*– pp. 4828-4834.

Stevens, S. H., V. A. Kuuskraa, and J. Gale (2000), Sequestration of CO_2 in depleted oil and gas fields: global capacity, costs and barriers, in *Proceedings of the 5th International Conference on Greenhouse Gas Control Technologies (GHGT-5), DJ Williams, RA Durie, P. McMullan, CAJ Paulson and AY Smith (eds.)*, pp. 13–16.

Thompson, P.J. and P.D. Butcher (1991), The geology and geophysics of the Everest Complex. In: Spencer, A.M. (ed). Generation, accumulation and production of Europe's hydrocarbons. Special publication of the European Association of Petroleum Geoscientists No. 1, pp. 89-98. Oxford University Press, Oxford. The European Association of Petroleum Geoscientists.

Whyatt, M., J. Bowen, and D. Rhodes (1992), The Nelson Field: a successful application of a development geoseismic model in North Sea exploration, *Geological Society, London, Special Publications*, *67*(1), 283–305.

Wildenborg, T., H. Dudok van Heel and F. Van Bergen (2003), CO_2 Storage Potential of Saline Aquifers in the Netherlands Onshore Region. Study Area A, Southern North Sea, Netherlands Institute of Applied Geoscience TNO – National Geological Survey, Utrecht.

Wills, J. (1991), The Forties Field, Block 21/10, 22/6a, UK North Sea, *Geological Society, London, Memoirs*, *14*(1), 301–308.

Zhou, Q., J. T. Birkholzer, C.-F. Tsang, and J. Rutqvist (2008), A method for quick assessment of CO_2 storage capacity in closed and semi-closed saline formations, *International Journal of Greenhouse Gas Control*, *2*(4), 626–639.

Yamamoto, H., K. Zhang, K. Karasaki, A. Marui, H. Uehara, and N. Nishikawa (2009), Numerical Investigation Concerning the Impact of CO_2 Geologic Storage on Regional Groundwater Flow. *International Journal of Greenhouse Gas Control* 3 (5). Elsevier: 586–99.